Eur. Phys. J. B **10**, 45–52 (1999)

THE EUROPEAN PHYSICAL JOURNAL B

EDP Sciences

Interfacial roughness in a near-critical binary fluid mixture: X-ray reflectivity and near-specular diffuse scattering

B.R. McClain[a], M. Yoon[b], J.D. Litster, and S.G.J. Mochrie

Department of Physics, Massachusetts Institute of Technology, Cambridge, Massachusetts 02139-4307, USA

Received 1 April 1998

Abstract. Measurements are presented of the X-ray specular reflectivity and near-specular diffuse scattering of the interface in a near-critical mixture of hexane and perfluorohexane. A lineshape analysis of the scattered intensity at each temperature yields values for the interfacial tension and interfacial width. The temperature variation of the tension and width so-obtained are consistent with current understanding of this interface, which holds that there is, firstly, an intrinsic width over which the fluid density varies smoothly from one coexistence composition to the other, and, secondly, that the interface acquires an additional and larger statistical interfacial width as a result of capillary fluctuations.

PACS. 82.70.Dd Colloids – 42.25.Kb Coherence

1 Introduction

The character of the interface in a binary fluid mixture near its consolute point remains a topic of longstanding interest [1–8]. Current understanding of this interface holds that there is, firstly, an intrinsic width over which the fluid density varies smoothly from one coexistence composition to the other, and, secondly, that the interface acquires an additional statistical interfacial width as a result of capillary fluctuations. Both contributions to the interfacial width increase dramatically as the temperature increases towards the consolute point, where the interface ceases to exist.

In previous experimental work on this topic, the role of capillary fluctuations in roughening and broadening the interface was inferred from their effect on the specular reflectivity and ellipticity of light reflected from the interface in question. In particular, the interfacial width, determined from measurements of the specular reflectivity, was considerably larger than could be accounted for based on theoretical calculations of the intrinsic width alone. In the present paper, we describe measurements of the X-ray specular reflectivity carried out to determine the interfacial width in a near-critical binary fluid mixture of hexane and perfluorohexane [9]. We simultaneously measured the near-specular X-ray diffuse scattering originating in lateral inhomogeneities of the interface, due to capillary excitations. Our measurements directly confirm the existence of large-amplitude capillary modes at the interface. The observed intensities of the diffuse and specular scattering allow us to determine the interfacial tension and interfacial width by means of a comparison to model profiles, parameterized by these quantities, and then least-mean-squares fit to the experimental data. Our fitting results are consistent with an interfacial tension that varies as the reduced temperature raised to the power $2\nu = 1.26$, where ν is the correlation length exponent of the three dimensional (3D) Ising universality class [10]. The fitting results also confirm that as a practical matter the major contribution to the measured interfacial width of a near-critical interface is a result of interface roughness due to capillary modes. However, they do indicate the existence of an additional intrinsic contribution to the total interface width. On the technical side, these experiments further demonstrate the utility of X-ray techniques for the investigation of interfacial, and not only surface, morphology.

2 Theoretical background

2.1 Interfacial roughness

A nominally flat and smooth fluid interface at thermal equilibrium will be subject to thermal fluctuations – that is, there will be capillary modes – and consequently the interface will acquire a certain roughness [2]. In this section, we review the derivation of approximate expressions for the root-mean-square (rms) roughness and also for certain related correlation functions. Our approach follows that of reference [11] and references therein.

[a] *Present address*: Department of Molecular and Cellular Biology, Harvard University, Cambridge, MA 02138, USA.
e-mail: `mcclain@xtal200.harvard.edu`

[b] *Present address*: Solid State Division, Oak Ridge National Laboratory, Oak Ridge, TN 37831, USA.

The interfacial energy is given by

$$H = \int \mathrm{d}^2\mathbf{r} \left\{ \gamma\sqrt{1+(\nabla h)^2} + \frac{g\rho}{2}h^2 \right\}, \qquad (1)$$

where $\mathbf{r} = (x, y)$, h is the deviation of the interfacial height from its equilibrium location (taken to be at $z = 0$), γ is the interfacial tension, g is the gravitational acceleration, and ρ is the difference in density between the fluid on either side of the interface. The first term is energy due to the interfacial area, and second term is a gravitational energy assuming that the interface is on-average horizontal. On the basis of an approximate mode-coupling calculation for an interface between simple fluids, Meunier [12] has suggested that equation (1) may be satisfactorily represented as

$$H = \int \mathrm{d}^2\mathbf{r} \left\{ \frac{\gamma}{2}(\nabla h)^2 + \frac{g\rho}{2}h^2 + \frac{\kappa}{2}(\nabla^2 h)^2 \right\}, \qquad (2)$$

where $\kappa = 3k_\mathrm{B}T/8\pi$ is an effective bending rigidity. Applying the equipartition theorem to equation (2), it follows that

$$\langle |h_\mathbf{q}|^2 \rangle = \frac{k_\mathrm{B}T/A}{\gamma q^2 + g\rho + \kappa q^4}, \qquad (3)$$

where $\mathbf{q} = (Q_x, Q_y)$, $q = |\mathbf{q}|$, A is the interfacial area, and $h_\mathbf{q}$ is the amplitude of the capillary mode of wavevector $\mathbf{q}$, so that

$$h(\mathbf{r}) = \frac{A}{2\pi}\int \mathrm{d}^2\mathbf{q} h_\mathbf{q} \mathrm{e}^{\mathrm{i}\mathbf{q}\cdot\mathbf{r}}. \qquad (4)$$

Of particular relevance to the present paper is the height-height correlation function $[g(r)]$, which is given by

$$g(r) = \langle h(\mathbf{r})h(\mathbf{0})\rangle = \frac{A}{4\pi^2}\int \mathrm{d}^2\mathbf{q}\langle |h_\mathbf{q}|^2\rangle \cos(\mathbf{q}\cdot\mathbf{r}). \qquad (5)$$

The integral of equation (5) may be evaluated in closed form as follows:

$$\begin{aligned} g(r) &= \frac{k_\mathrm{B}T}{4\pi^2}\int_0^\infty \frac{q\mathrm{d}q}{\kappa q^4 + \gamma q^2 + g\rho}\int_0^{2\pi}\cos(qr\cos\varphi)\mathrm{d}\varphi \\ &= \frac{k_\mathrm{B}T}{2\pi}\int_0^\infty \frac{qJ_0(qr)\mathrm{d}q}{\kappa q^4 + \gamma q^2 + g\rho} \\ &= \frac{k_\mathrm{B}T}{2\pi\sqrt{\gamma^2 - 4g\rho\kappa}}\int_0^\infty qJ_0(qr)\mathrm{d}q \\ &\quad\times\left[\frac{1}{q^2 + \frac{\gamma - \sqrt{\gamma^2-4g\rho\kappa}}{2\kappa}} - \frac{1}{q^2 + \frac{\gamma + \sqrt{\gamma^2-4g\rho\kappa}}{2\kappa}}\right] \\ &= \frac{k_\mathrm{B}T}{2\pi\sqrt{\gamma^2 - 4g\rho\kappa}} \\ &\quad\times\left[K_0\left(r\sqrt{\frac{\gamma - \sqrt{\gamma^2-4g\rho\kappa}}{2\kappa}}\right)\right. \\ &\quad\left. - K_0\left(r\sqrt{\frac{\gamma + \sqrt{\gamma^2-4g\rho\kappa}}{2\kappa}}\right)\right], \end{aligned} \qquad (6)$$

where J is the Bessel function and K is the modified Bessel function. From the height-height correlation function, we may obtain the mean square interfacial roughness ($\sigma^2 = g(0)$) as

$$\sigma^2 = \frac{k_\mathrm{B}T}{2\pi\sqrt{\gamma^2 - 4g\rho\kappa}}\ln\sqrt{\frac{\gamma + \sqrt{\gamma^2-4g\rho\kappa}}{\gamma - \sqrt{\gamma^2-4g\rho\kappa}}}\,. \qquad (7)$$

(For small arguments $K_0(z) \simeq -\ln z + 0.11593$.)

Equation (7) may be written more economically if we define $\zeta \equiv \sqrt{\kappa/\gamma}$, which may be interpreted as the shortest wavelength for capillary modes, and $L_\mathrm{g} \equiv \sqrt{\gamma/g\rho}$, which is the capillary length. In terms of these quantities and further introducing $s \equiv \sqrt{1 - 4(\zeta/L_\mathrm{g})^2}$, the height-height correlation function may be written

$$g(r) = \frac{k_\mathrm{B}T}{2\pi\gamma s}\left[K_0\left(\frac{r}{\zeta}\sqrt{\frac{1-s}{2}}\right) - K_0\left(\frac{r}{\zeta}\sqrt{\frac{1+s}{2}}\right)\right], \qquad (8)$$

and the mean square roughness may be written

$$\sigma^2 = \frac{k_\mathrm{B}T}{2\pi\gamma s}\ln\sqrt{\frac{1+s}{1-s}}\,. \qquad (9)$$

In passing, it is worth noting that these expressions may be useful in the case of thin films on a substrate, where the van der Waals interaction between the film and the substrate tends to suppress fluctuations in just the same way as gravity, so that $L_\mathrm{g} = \sqrt{2\pi\gamma d^4/A}$, where d is the film thickness, and A is the appropriate Hamaker constant [13].

It is evident that equations (8, 9) are only sensible for $L_\mathrm{g} > 2\zeta$. In reality, L_g is usually much larger than ζ, so that

$$g(r) \simeq \frac{k_\mathrm{B}T}{2\pi\gamma}\left[0.11593 - K_0\left(\frac{r}{\zeta}\right) - \ln\left(\frac{r}{L_\mathrm{g}}\right)\right] \qquad (10)$$

$$\sigma^2 \simeq \frac{k_\mathrm{B}T}{2\pi\gamma}\ln\left(\frac{L_\mathrm{g}}{\zeta}\right). \qquad (11)$$

2.2 Near-critical fluid interface

In this section, we briefly review the properties of near-critical fluid mixtures and of the interface between them in the neighborhood of their consolute point at a critical temperature of T_c and critical density ρ_c, where the interface ceases to exist. The difference in density, between the two phases is $\rho = A\rho_\mathrm{c}t^\beta$, where A is a constant, $t = (T_\mathrm{c} - T)/T_\mathrm{c}$ is the reduced temperature, and $\beta \simeq 0.32$ is the order-parameter critical exponent for the universality class of the 3D Ising model. Near the consolute point, it is generally accepted that the interfacial tension varies as the inverse square of the correlation length, *i.e.* $\gamma = Bk_\mathrm{B}T_\mathrm{c}/\xi^2 = Bk_\mathrm{B}T_\mathrm{c}t^{2\nu}/\xi_0^2$, where $\xi = \xi_0 t^{-\nu}$ is the bulk correlation length below T_c, and $\nu = 0.63$ is the 3D Ising correlation length exponent. Moreover, according to to the principle of two-scale factor universality, $B \simeq 0.10$ is a universal constant

[14,15]. It follows that $\zeta = \sqrt{(3/8\pi B)}\xi_0 t^{-\nu} = 1.09\xi_0 t^{-\nu}$ and $L_g = \sqrt{(Bk_B T_c/gA\rho_c\xi_0^2)}t^{\nu-\beta/2}$.

According to reference [4], the intrinsic interfacial density profile in the direction perpendicular to the interface (z) is well approximated by

$$\rho_1(z) = \frac{(\rho_1+\rho_2)}{2} + \frac{(\rho_1-\rho_2)}{2}\frac{\sqrt{2}\tanh(z/2\xi)}{\sqrt{3-\tanh^2(z/2\xi)}}, \quad (12)$$

where ξ is the bulk correlation length, and ρ_1 and ρ_2 are the densities of the coexisting phases. It turns out that equation (12) is numerically close to an error function with a one-sigma width of $w \simeq 2\xi$ [3], *i.e.*

$$\rho_1(z) \simeq \frac{(\rho_1+\rho_2)}{2} + \frac{(\rho_1-\rho_2)}{2}\mathrm{erf}(z/\sqrt{2}2\xi). \quad (13)$$

The form of the mean density profile produced by capillary fluctuations is an error function. The statistical one-sigma width of interfacial density profile may be written using the expressions given above as $\sigma = 1.26\xi\sqrt{\ln(L_g/\zeta)}$. Usually, L_g/ζ will be large, so that σ may be expected to be several times ξ. For example, using the values of ρ and γ presented below in Sections 4.1 and 4.2, respectively, we find for near-critical hexane-perfluorohexane mixtures that $\log(L_g/\zeta) \simeq \log(6.27\times10^6) + 1.1\log(t) \simeq 12.3$ (9.7) and $\sigma \simeq 4.4\xi$ (3.9ξ) at a reduced temperature of 0.05 (0.005). Under these circumstances, the dominant contribution to the total interfacial width is expected to be associated with capillary modes. It should be noted however that ζ diverges while L_g vanishes as the consolute point is approached. It follows that the discussion of Section 2.1 breaks down very close to but below T_c.

2.3 X-ray scattering from an interface

The X-ray scattering from an on-average flat and abrupt interface, separating fluid medium 1 from fluid medium 2, consists of a specularly reflected component and a diffuse component. Expressions for the specular and diffuse components within the distorted-wave Born approximation in terms of the interfacial roughness and the height-difference correlation function have been given in reference [16]. It is worthwhile emphasizing that two aspects of the present experiment facilitate the separation of the specular and diffuse scattering: first, the especially low interfacial tension near a consolute point renders the diffuse scattering of larger intensity and of greater width (because of the smaller capillary length) than in the more usually studied case of a fluid-vapor interface. The second factor is the very fine angular resolution that we employed within the scattering plane.

The specular reflectivity for X-rays incident (and reflected) at an angle α is

$$R(\alpha) = R_F(\alpha)\mathrm{e}^{-\sigma^2 Q_z Q_z^t}, \quad (14)$$

where

$$R_F(\alpha) = \left|\frac{\sin\alpha - \sqrt{(n_2/n_1)^2 - 1 + \sin^2\alpha}}{\sin\alpha + \sqrt{(n_2/n_1)^2 - 1 + \sin^2\alpha}}\right|^2, \quad (15)$$

is the Fresnel reflectivity of an interface separating media of refractive indices n_1 and n_2, respectively, $Q_z = k_1(\sin\alpha + \sin\beta)$ is the scattering wavevector in medium 1 (k_1 is the X-ray wavenumber in medium 1 and β is the scattering angle with respect to the interface), and

$$Q_z^t = k_1\left[\sqrt{\sin^2\alpha + \frac{n_2^2}{n_1^2} - 1} + \sqrt{\sin^2\beta + \frac{n_2^2}{n_1^2} - 1}\right]$$

is the wavevector in medium 2. It is worth noting that for X-radiation propagating in a medium (medium j) containing only elements of relatively low atomic number, as in the present experiment, the refractive index is $n_j = 1 - \delta_j - \mathrm{i}\epsilon_j$, with $\delta_j = r_0\lambda_j^2\rho_j/2\pi$ and $\epsilon_j = \lambda_j/4\pi\Lambda_j$, where r_0 is the Thomson radius of the electron, λ_j is the X-ray wavelength in medium j, ρ_j is the electron density of medium j, and Λ_j is the X-ray absorption length in medium j. The critical angle for total external reflection is then $\alpha_c \simeq \sqrt{2(\delta_2 - \delta_1)} = \sqrt{r_0\lambda^2(\rho_2-\rho_1)/\pi}$.

We now turn to the diffuse scattering. In the present experiment the detector acceptance in the direction perpendicular to the scattering plane (the Q_y direction) is very large. It follows that the measured intensity is effectively an integral over Q_y. Therefore, the resultant intensity of near-specular diffuse scattering as a function of Q_x is predicted to be

$$I_D/I_O = \frac{T(\alpha)T(\beta)r_0^2\lambda_1(\rho_2-\rho_1)^2\mathrm{e}^{-\sigma^2[(\mathrm{Re}Q_z^t)^2-(\mathrm{Im}Q_z^t)^2]}}{\sin\alpha|Q_z^t|^2} \times \int_0^\infty \mathrm{d}x\mathrm{e}^{\mathrm{i}Q_x x}\mathrm{e}^{-x^2\Delta Q_x^2/16\ln 2}\left(\mathrm{e}^{|Q_z^t|^2 g(x)} - 1\right), \quad (16)$$

where I_D/I_O is the ratio of the diffuse to the incident intensities and

$$T(\alpha) = \left|\frac{2\sin\alpha}{\sin\alpha + \sqrt{\sin^2\alpha + (n_2/n_1)^2 - 1}}\right|^2 \quad (17)$$

is the Fresnel transmissivity of the interface, and $\Delta Q_x = Q_z\Delta\beta/2$, with $\Delta\beta$ the full-width-at-half-maximum of the detector angular acceptance within the scattering plane, which we take to be Gaussian. As discussed in reference [11], equation (16) displays no dependence on the horizontal detector acceptance because the scattering, although in principle diffuse, is sharply peaked while the horizontal acceptance is large, so that all scattered X-rays are collected.

So far in this section, we have supposed an abrupt interface, in which case equations (14, 16) supplemented by equations (8, 9) constitute a complete description

of the X-ray scattering. In this regard, it is notable that, assuming that the density difference between the coexisting phases is known, which will indeed be the case, the only quantity determining interfacial properties is the interfacial tension. For an interface possessing an additional intrinsic width (w), it is shown in reference [20] that we may continue to employ equations (14, 16), and to reinterpret σ as the total interfacial width, including the intrinsic width as well as the statistical width, *i.e.*

$$\sigma^2 = w^2 + \frac{k_{\rm B}T}{2\pi\gamma} \ln\left(\frac{L_{\rm g}}{\zeta}\right). \tag{18}$$

Supposing that $w = \tilde{w}\xi$, where $\tilde{w}$ is a constant, we may express the total interfacial width as

$$\sigma = \xi\sqrt{\tilde{w}^2 + 1.58\ln(L_{\rm g}/\zeta)}. \tag{19}$$

As discussed above, we may expect $\tilde{w} \simeq 2$.

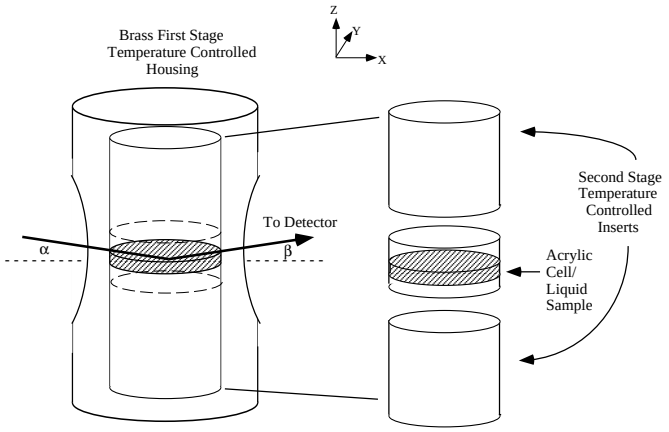

Fig. 1. Experimental setup for measuring the X-ray scattering from a binary fluid interface. The incoming and outgoing X-ray beams are in the $X-Z$ plane and at angles α and β from the horizontal interface.

3 Experimental methods

Measurements of the X-ray reflectivity and near-specular diffuse scattering have emerged as an important means to study the microscopic and mesoscopic structure through and across an interface. These techniques have been used, for example, to study capillary wave fluctuations at the vapor-liquid [11,17,18] and liquid-liquid interface [19]. There is in addition a substantial and rapidly growing literature describing the application of neutron reflectivity to polymer interfaces [21]. In order to apply X-ray methods to a near-critical liquid-liquid interface, we first had to overcome a number of problems.

One obstacle is the upper liquid phase itself which attenuates the incident and reflected X-ray beams. Following the experiments described in reference [19], this difficulty was similarly mitigated by using a relatively high X-ray energy in the present experiments, which is available at MIT-IBM beamline X20B at the National Synchrotron Light Source (NSLS). Specifically, we used X-rays of wavelength $\lambda = 0.714$ Å, corresponding to an energy of 17.4 keV.

Another problem is that using higher energy X-rays unavoidably reduces the critical angle for total external reflection, which is in any case small for a near critical interface, because the densities of the two coexisting phases approach each other as the consolute point is approached. Fortunately, the high X-ray brightness available at the NSLS allows highly collimated X-ray beams to be used. Nevertheless, to have as-large-as-possible a critical angle and to enhance the interfacial diffuse scattering as much as possible, we chose to examine the interface in mixtures of hexane (C_6H_{14}) and perfluorohexane (C_6F_{14}), which were found to exhibit a consolute point at $T_{\rm c} = 295.8$ K and $\rho_{\rm c} = 1.14$ gcm^{-3} in reference [9]. We used 98%-pure perfluorohexane from PCR Inc. of Gainsville, Florida, and 99.5%-pure hexane from Fluka without further purification. The densities of hexane and perfluorohexane are $\rho_{\rm H} = 0.659$ gcm^{-3} and 1.69 gcm^{-3}, respectively. The difference in their densities is therefore relatively large for fluid pairs exhibiting convenient consolute points. Even so, near the consolute point (which we found to occur at $T_{\rm c} = 295.17$ K and $\rho_{\rm c} = 1.141$ gcm^{-3}, in fair agreement with Ref. [9]) the critical angle is typically hundredths of degrees. At such low angles, in addition to fine angular resolution, it is also necessary to employ small beam dimensions, and relatively large sample areas, so as to contain the X-ray footprint within the sample area of interest. Possible complications associated with interfacial curvature near the walls of the cell indicate that a relatively large interfacial area should be used, in conflict with the requirement that the sample diameter not significantly exceed the X-ray absorption length. However, the small interfacial tension and consequently small capillary length ameliorate this problem somewhat in near critical mixtures. The absorption lengths of pure hexane and pure perfluorohexane are $\Lambda_{\rm H} = 3.00$ cm and $\Lambda_{\rm F} = 0.452$ cm, respectively.

The experimental setup is depicted in Figure 1. Except for the smaller sample cell and fine temperature control inserts, it is identical to that described in reference [19]. The incoming beam was tilted downward by an angle α using the Bragg reflection from a single Ge(111) crystal. The liquid sample was held in a cylindrical acrylic cell with polyvinylidene fluoride $[-(CF_2CH_2)_n-]$ windows in order to reduce preferential wetting, and thus meniscus, as much as possible. The inner diameter of the sample cavity was 2.5 cm, and to reduce mechanically induced interfacial vibrations its height was 1 mm [22]. This cell was placed in a brass housing which provided rough temperature control (± 0.1 K). Fine temperature control (± 0.005 K) was provided by a pair of Peltier heat pumps located close to the sample cell. This assembly was located on a vertical stage which was adjusted, depending on the incidence angle, such that the incoming beam always hit the center of the interface. The detector was located on a second vertical stage and was adjusted so that the signal

scattered at the desired angle β was sampled. A pair of slits located just before the sample was used to define the vertical (5 μm) and horizontal (1 mm) widths of the beam and thus the illuminated sample area. With this configuration, the beam footprint on the sample at the critical angle was small enough to reside completely on the fluid-fluid interface, even at the smallest angles studied. A second pair of slits placed just before the detector defined the vertical angular acceptance to be 2×10^{-5} radians while leaving the horizontal angular acceptance essentially wide open.

Attenuation of the X-ray beam provides one important benefit in that it allows a simple and convenient means for determining the phase diagram. Specifically, at each temperature the sample height was varied and the X-ray transmission through the two coexisting phases either side of the interface was measured, enabling the density of each phase to be deduced as a function of temperature. This is accomplished as follows. The fraction of X-rays transmitted through phase j (P_j) is related to the X-ray attenuation length (Λ_j) and the thickness of the sample cell (d) *via*

$$P_j = \mathrm{e}^{-d/\Lambda_j}. \tag{20}$$

It is then straightforward to show that the volume fraction of perfluorohexane in phase j is

$$f_j = \frac{-\ln P_j/d - \Lambda_{\mathrm{H}}^{-1}}{\Lambda_{\mathrm{F}}^{-1} - \Lambda_{\mathrm{H}}^{-1}}, \tag{21}$$

so that the density of phase j may be deduced as

$$\rho_j = f_j\rho_{\mathrm{F}} + (1 - f_j)\rho_{\mathrm{H}}. \tag{22}$$

Using the values of ρ_j and Λ_j measured at each temperature, the X-ray refractive index of phase j may be determined at each temperature.

4 Results and discussion

4.1 Phase diagram

The hexane-perfluorohexane phase diagram, deduced from the X-ray transmission of each coexisting phase, is shown in Figure 2 *versus* temperature and density. The solid circles are the measured densities. These data are not sufficiently numerous or accurate to improve upon earlier values for 3D Ising critical exponents. Therefore, we have chosen to employ the literature 3D Ising critical exponents to describe the data shown here and elsewhere in this paper [10]. Specifically, the solid line is given by

$$\rho_j = \rho_{\mathrm{c}}(1 \pm 0.5At^{\beta} + Ct^{1-\alpha}) \tag{23}$$

where $t = (T_{\mathrm{c}} - T)/T_{\mathrm{c}}$ is the reduced temperature, $\alpha = 0.11$ and $\beta = 0.32$ are the specific heat and order parameter exponents, respectively, of the 3D Ising model and $T_{\mathrm{c}} = 295.17 \pm 0.04$ K, $\rho_{\mathrm{c}} = 1.141 \pm 0.001$ g cm^{-3}, $A = 1.899 \pm 0.004$ and $C = 0.51 \pm 0.05$ are the best values determined by least-mean-squares fitting. Evidently, the data are well-described by equation (23).

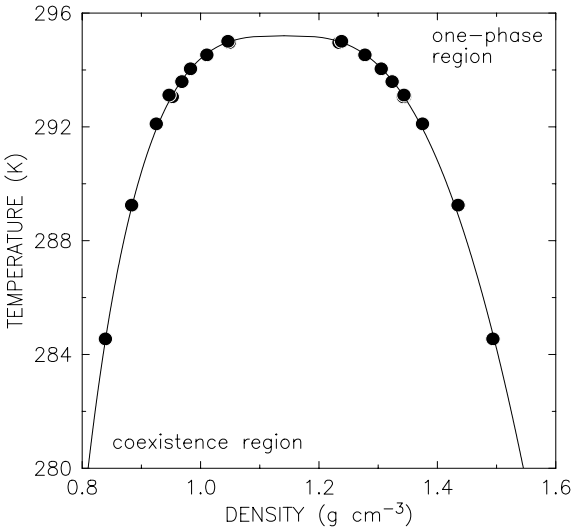

Fig. 2. Phase diagram of hexane-perfluorohexane near the consolute point. Solid circles are data points. The solid line is the model discussed in the text.

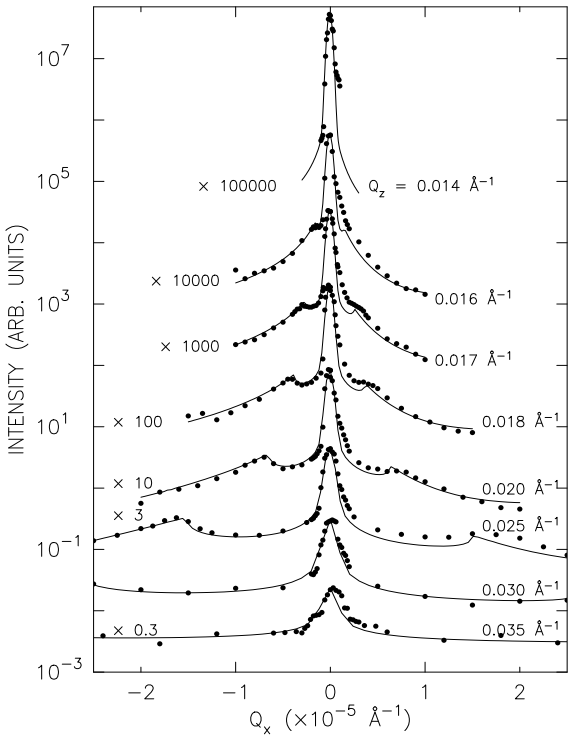

Fig. 3. Measured intensity (circles) *versus* Q_x for several values of Q_z obtained at 286.7 K. The line is the model form described in the text.

4.2 Interfacial tension

In Figure 3 are profiles showing the observed scattering *versus* Q_x for several values of Q_z, obtained at 286.7 K. In each profile, the peak at $Q_x = 0$ corresponds to specularly reflected X-rays. The shape and width of this peak are determined by the instrumental angular acceptance and by the interfacial flatness. In particular, we ascribe the asymmetry of the specular peak in Figure 3 to a slight

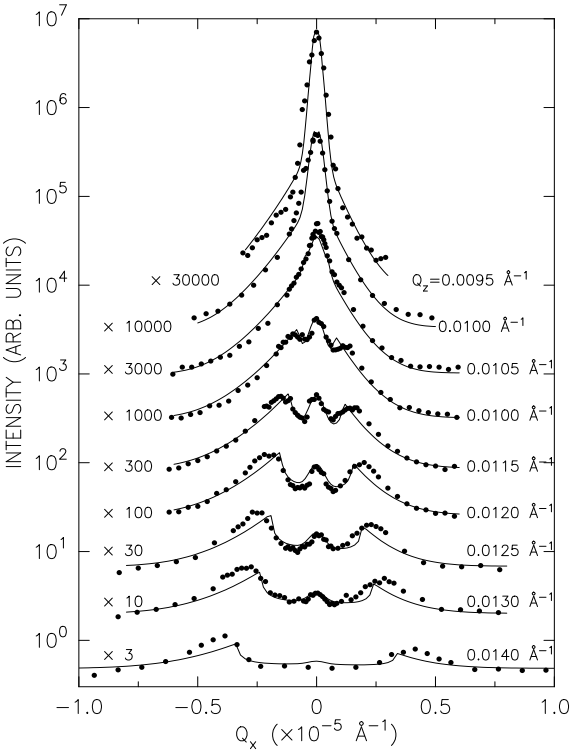

Fig. 4. Measured intensity (circles) *versus* Q_x for several values of Q_z obtained at 293.5 K. The line is the model form described in the text.

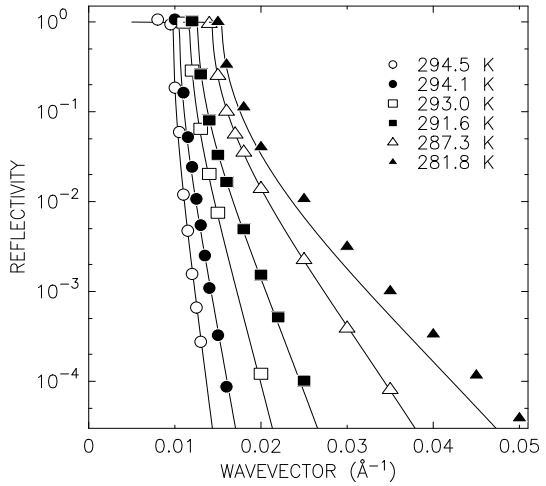

Fig. 5. Specular reflectivity (symbols) *versus* Q_z for several temperatures below the consolute point at 295.17 K. The lines correspond to the model reflectivity described in the text.

curvature of the interface at this temperature. The intensity of the specular peak evidently decreases with increasing Q_z. Away from $Q_x = 0$, there is additional scattering intensity, which also decreases with increasing Q_z. This is diffuse scattering, which originates from interfacial roughness. With increasing Q_z, two peaks emerge symmetrically displaced from the specular location. The displacement of these peaks from the specular position increases with increasing Q_z. In fact, these well-known features, often called "Yoneda wings" [23], occur whenever the angle between the interface and the incident or reflected X-ray beam equals the critical angle for total external reflection. This is because the Fresnel transmissivity *versus* angle (Eq. (17)), which appears (twice) in the expression for the intensity of the diffuse scattering (Eq. (16)), exhibits a peak at the critical angle. The utility of this phenomenon in the present experiment is that it is an unambiguous signature of interfacial diffuse scattering as a result of capillary modes. In particular, the observed diffuse scattering is not the result of bulk critical fluctuations. (We may expect that there is scattering as a result of bulk fluctuations near the interface, which in principle will display Yoneda wings. However, this scattering is dominated by scattering from bulk fluctuations from the very much larger illuminated volume above and not adjacent to the interface, which would not show Yoneda wings. Consequently, the total of any scattering from bulk fluctuations will not show the Yoneda enhancement.)

Analogous data obtained at 293.5 K are displayed in Figure 4. Qualitatively, these data appear similar to those shown in Figure 3. There are important differences, however. The first is that the relative intensity of the diffuse scattering is larger in comparison to the specular scattering at 293.5 K than at 286.7 K, suggesting that the interfacial tension decreases as the consolute point is approached. Second, the specular peaks appear more symmetrical than at 286.7 K, corresponding to a flatter interface at this temperature as a result of the reduced interfacial tension. The specular peak width at each value of Q_z at this temperature corresponds to what is expected on the basis of the instrumental resolution. Third, the intensity of the specular scattering decreases much more rapidly with increasing Q_z at 293.5 K than at 286.7 K, indicating a larger interfacial width at the higher temperature. This behavior is highlighted in Figure 5, which collects the specular reflectivity measured *versus* Q_z at several temperatures. In each of these profiles, the reflectivity is near unity for wavevectors corresponding to incidence angles less that the critical angle for total external reflection. The decrease in the critical angle with increasing temperature corresponds to the decreasing density difference between the two coexisting phases as the consolute point is approached. At larger wavevectors, the reflectivity decreases rapidly. As expected, the fall-off is increasingly rapid at increasingly higher temperatures. It is apparent in Figure 4 that the model underestimates the width of the peak of the Yoneda wings. We do not understand this observation quantitatively. However, we note that the interfacial roughness near the consolute point is unusually large. To the contrary, the form of the Fresnel transmissivity, which gives rise to the Yoneda wings, is predicated on a flat interface. It is therefore perhaps not surprising that there is a discrepancy.

In order to determine the variation of the interfacial width and tension with temperature, we fitted the profiles obtained at 286.7 K (Fig. 3), at 293.5 K (Fig. 4), and at several additional temperatures (data not shown)

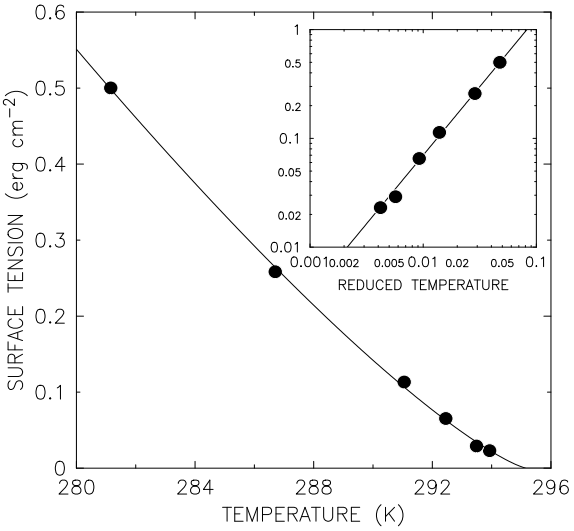

Fig. 6. Best fit values of the interfacial tension (circles) at several temperatures below the consolute point plotted on a linear scale. Inset: interfacial tension plotted *versus* reduced temperature on a log-log scale. Solid lines correspond to a model power-law form with the exponent fixed at the expected value of 1.26, as described in the text.

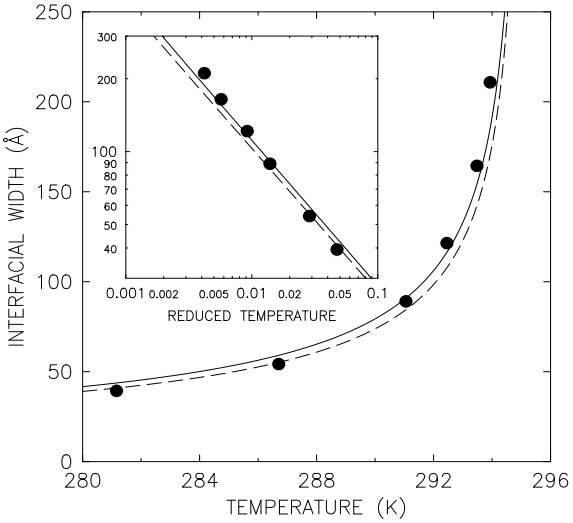

Fig. 7. Best fit values of the interfacial width (circles) at several temperatures below the consolute point plotted on a linear scale. Inset: interfacial width *versus* reduced temperature plotted on a log-log scale. Dashed lines correspond to the expected statistical interfacial width (Eq. (11)). Solid lines correspond to the best fit to equation (19).

to the model form

$$I/I_0 = R\mathrm{e}^{-Q_x^2 4\ln 2/\Delta Q_x^2} + I_\mathrm{D}/I_0 + B, \qquad (24)$$

where R and I_D are given by equations (14, 16), respectively, and B represents background scattering, which was taken to be independent of Q_x but not independent of Q_z. Equation (24) was considered a function of Q_x and Q_z and for each temperature a single fit was carried out, involving all of the profiles obtained at that temperature. For each temperature studied, the quantities varied in the fits were γ, σ and four parameters to describe the background. The densities of each phase were determined by measuring their respective X-ray transmissions, as described above, and were not varied in the fits. The resultant best fit profiles are shown as the lines in Figures 3 and 4. The fits provide a good description of the data over the whole range of wavevectors studied and at both temperatures.

The solid lines in Figure 5 correspond to the model for the specular reflectivity plotted with the best fit parameters. That the critical angle is accurately located at every temperature confirms that the density difference between the phases was determined correctly.

The best fit values of the interfacial tension obtained at several temperatures below the consolute point are plotted in Figure 6. The inset reproduces these results on a log-log scale. It is apparent that the interfacial tension decreases rapidly with increasing temperature, changing by a factor of more than twenty over the range of temperatures studied. As noted above, the interfacial tension is expected to vary as $\gamma = (Bk_\mathrm{B}T_\mathrm{c}/\xi_0^2)t^{2\nu}$, where $\nu = 0.63$ is the correlation length exponent and $B = 0.1$ is a universal constant. Fitting our results for the interfacial tension to such a power law gives $Bk_\mathrm{B}T_\mathrm{c}/\xi_0^2 = 23.2 \pm 0.8$ erg cm^{-2}, which is shown as the solid lines in Figure 6. Clearly, the model provides an excellent description of the experimental data. We may deduce that $\xi_0 = 1.32$ Å.

As far as we are aware, measurements of the correlation length for the hexane-perfluorohexane system are presently not available. An independent measurement of ξ_0 – using small-angle X-ray scattering techniques, for example – would serve to confirm (or refute) that $B \simeq 0.1$ for hexane-perfluorohexane mixtures. However, there are published values for the correlation length above T_c in comparable systems [24]. In particular, Calmetter *et al.* [25] studied a critical mixture of aniline and cyclohexane, for which the mean volume per particle at the critical composition is not very different from that of critical hexane-perfluorohexane mixtures. Calmetter *et al.* found that $\xi = (2.2 \pm 0.1$ Å$)t^{-0.63}$ above T_c. That their exponent for the correlation length is the same as used here further facilitates comparison. The ratio of correlation lengths above and below T_c is a universal constant equal to 1.96 for the 3D Ising model [10]. Therefore, below T_c, we may expect the correlation length for the analine-cyclohexane mixture to be $\xi = (1.1$ Å$)t^{-0.63}$, which is certainly similar to the value deduced in the present paper for hexane-perfluorohexane below T_c.

Shown in Figure 7 are the corresponding best fit values of the interfacial width (σ), which evidently increases by a factor of more than five from the lowest to the highest temperature studied. We may compare these measurements to the statistical interfacial width predicted from the measured interfacial tension *via* equation (11). This is shown as the dashed line in the figure. Evidently, the statistical width alone systematically underestimates the measured interfacial width near T_c. We have therefore fit these data to equation (19) with $\tilde{w}$ as the only variable parameter. The result, corresponding to $\tilde{w} = 1.7 \pm 0.5$,

is shown as the solid line and provides a fair description of the measured interfacial width. However, it may be seen that the variation of the measured width *versus* reduced temperature appears more rapid than predicted by the model. The origin of this behavior is uncertain. Nevertheless, the best fit value of $\tilde{w}$ is consistent with the expectation that $\tilde{w} \simeq 2$ [4]. Although the theoretical variation of the interfacial width with reduced temperature deviates from a power law by virtue of its dependence on $\log(L_g/\zeta)$, the deviation of the model from a straight line in the inset of Figure 7 – that is, from a power law of 0.63 – is imperceptible.

5 Conclusion

We have carried out measurements of the X-ray specular reflectivity and near-specular diffuse scattering of the interface in a near-critical mixture of hexane and perfluorohexane. A lineshape analysis of the scattered intensity at each temperature yields values for the interfacial tension and width. The temperature variation of the interfacial tension and width so-obtained are quantitatively consistent with theoretical predictions. Finally, we may note that the present experiment further demonstrates the potential for X-ray-based investigations of a myriad of interfacial phenomena, including those associated with critical points [26], critical end points [27], wetting and prewetting [28–30], and the behavior of polymers at interfaces [31]. The increasing availability of high-brightness, high-energy X-ray beams (which have significantly reduced adsorption compared to lower-energy X-ray beams) at the new, high-energy, third-generation synchrotrons – the European Synchrotron Radiation Facility, the Advanced Photon Source, and SPring-8 – will facilitate this program.

We are grateful to Bruce Carvalho and Dan Lee for many valuable discussions. S. G. J. M. thanks Profs. J. Higgins and P. Luckham of Imperial College, London, for their hospitality. This work was support by the NSF (DMR-9423641). Beamline X20B is supported in part by the NSF (DMR-9400333). The NSLS is supported by the DOE (DE-AC0276CH00016).

References

1. G.H. Gilmer, W. Gilmore, J. Huang, W.W. Webb, Phys. Rev. Lett. **14**, 491 (1965).
2. F.P. Buff, R.A. Lovett, F.H. Stillinger Jr., Phys. Rev. Lett. **15**, 621 (1965).
3. J. Huang, W.W. Webb, J. Chem. Phys. **50**, 3677 (1969).
4. S. Fisk, B. Widom, J. Chem. Phys. **50**, 3219 (1969).
5. D. Beaglehole, Physica A **112**, 320 (1982).
6. D.B. Abraham, Phys. Rev. B **25**, 4922 (1982).
7. J.V. Sengers, J.M.J. van Leeuwen, J.W. Schmidt, Physica A **172**, 20 (1991).
8. J.W. Schmidt, Physica A **172**, 40 (1991).
9. R.G. Bedford, R.D. Dunlop, J. Am. Chem. Soc. **80**, 282 (1958).
10. A.J. Liu, M.E. Fisher, Physica A **156**, 35 (1989).
11. M.K. Sanyal, S.K. Sinha, K.G. Huang, B.M. Ocko, Phys. Rev. Lett. **66**, 628 (1991).
12. J. Meunier, J. Phys. France **48**, 1819 (1987).
13. M. Sferrazza, C. Xiao, R.A.L. Jones, D.G. Bucknall, J. Webster, J. Penfold, Phys. Rev. Lett. **78**, 3693 (1997).
14. D. Stauffer, M. Ferrer, M. Wortis, Phys. Rev. Lett. **29**, 345 (1972).
15. V. Privman, P.C. Hohenberg, A. Aharony, in *Phase Transitions and Critical Phenomena*, edited by C. Domb, J.L. Lebowitz (Academic Press, London and Orlando, 1991), Vol. 14.
16. S.K. Sinha, E.B. Sirota, S. Garoff, H.B. Stanley, Phys. Rev. B **38**, 2297 (1988).
17. A. Braslau, M. Deutsch, P.S. Pershan, A.H. Weiss, J. Als-Nielsen, J. Bohr, Phys. Rev. Lett. **54**, 114 (1985).
18. A. Braslau, P.S. Pershan, G. Swislow, B.M. Ocko, J. Als-Nielsen, Phys. Rev. A **38**, 2457 (1988).
19. B.R. McClain, D.D. Lee, B.L. Carvalho, S.G.J. Mochrie, S.H. Chen, J.D. Litster, Phys. Rev. Lett. **72**, 246 (1994).
20. M.P. Gelfand, M.E. Fisher, Physica A **166**, 1 (1990).
21. D.G. Bucknall, J.S. Higgins, Rutherford-Appleton Laboratory Technical Report RAL-TR-97-008 (1997), for a comprehensive review.
22. C.A. Helm, H. Mohwald, K. Kjaer, J. Als-Nielsen, Biophys. J. **52**, 381 (1987).
23. Y. Yoneda, Phys. Rev. **131**, 2010 (1963).
24. H.L. Swinney, D.L. Henry, Phys. Rev. A **8**, 2586 (1973).
25. P. Calmetter, I. Lagües, C. Laj, Phys. Rev. Lett. **28**, 478 (1972).
26. M.E. Fisher, P.-G. de Gennes, C. R. Acad. Sci. Paris B **287**, 207 (1978).
27. M.E. Fisher, P.J. Upton, Phys. Rev. Lett. **65**, 3405 (1990).
28. E. Cheng, M. Cole, W.F. Saam, J. Treiner, Phys. Rev. Lett. **67**, 1007 (1991).
29. J. Rutledge, P. Taborek, Phys. Rev. Lett. **69**, 937 (1992).
30. E. Cheng, G. Mitsura, H.C. Lee, H.W.M. Chan, M.W. Cole, C. Carraro, W.F. Saam, F. Toigo, Phys. Rev. Lett. **70**, 1854 (1993).
31. G.J. Fleer, M.A. Cohen Stuart, J.M.H.M. Scheutjens, T. Cosgrove, B. Vincent, *Polymers at Interfaces* (Chapman and Hall, London, 1993).